6th European Conference on Computational Mechanics (ECCM 6)
7th European Conference on Computational Fluid Dynamics (ECFD 7)
11–15 June 2018, Glasgow, UK

A HYBRID APPROACH FOR CONSIDERATION OF THE ELASTIC-PLASTIC BEHAVIOUR OF OPEN-CELL CERAMIC FOAMS

CHRISTOPH SETTGAST[1,*], GERALF HÜTTER[1], MARTIN ABENDROTH[1] AND MEINHARD KUNA[1]

[1] Institute of Mechanics and Fluid Dynamics, TU Bergakademie Freiberg, Lampadiusstraße 4, 09599 Freiberg, Germany

Christoph.Settgast@imfd.tu-freiberg.de, Geralf.Huetter@imfd.tu-freiberg.de, Martin.Abendroth@imfd.tu-freiberg.de, Meinhard.Kuna@imfd.tu-freiberg.de

web page: http://tu-freiberg.de/fakult4/imfd/fkm

Key words: Open-cell foam, Elastic-plastic deformation, Constitutive modelling, Neural network

Abstract. Open-cell ceramic foams are used as filters during casting processes to reduce the non-metallic inclusions and the turbulence of the metal flow. Based on that, these foams have to withstand high temperature loadings and so elastic-plastic deformations can occur. The macroscopic elastic deformation behaviour of such foam structures was investigated and described successful in the literature. However, the plastic deformation behaviour strongly depends on the micro-structure and bulk material plasticity.

The current work presents a homogenized material model based on an adapted yield function to describe the elastic-plastic deformation behaviour of open-cell foam structures. The form of the yield function is not specified completely a priori. The specific shape is interpolated between results of finite element (FE) simulations of cell models using neural networks.

This modelling approach is proved for simple plasticity models, e.g. von Mises and Drucker-Prager, and further applied to an exemplary foam structure as a representative volume element (RVE) using a simple bulk material plasticity. The proposed model shows a good accordance for all tested elastic-plastic load cases and a reduction of the numerical effort by a factor of ≈ 200 for the simulation of the used simple foam structure.

1 INTRODUCTION

Within the collaborative research centre CRC 920 "Multi-functional filter for Metal Metal Filtration – A Contribution towards Zero Defect Materials" at the TU Bergakademie Freiberg, Germany, multifunctional open-cell foam filters, made of ceramic, are investigated to reduce the amount of non-metallic inclusions and turbulence of metal flow. Due to the high temperatures of the melt, no sufficient experimental observations can be performed on the foam, whereas numerical simulations of this process are necessary to

evaluate the integrity of the filter during the casting process. However, previous investigations indicated a plastic behaviour of the foam at temperatures in the range of the molten metal, cf. Solarek et al. [1]. The chemical composition and manufacturing process, e.g. coking temperature, have a great influence to the material properties, cf. Soltysiak et al. [2].

Using finite element (FE) simulations of fully discretized structures, several researchers investigated the elastic and plastic deformation behaviour of foams. The foam structure (topology and geometry) has a great influence on the yield surface [3] and on the elastic behaviour [4] of the foam. Additionally, the plastic deformation behaviour strongly depends on the micro-structure and the bulk material plasticity, cf. Wang and McDowell [3] and Demiray et al. [5], respectively.

Storm et al. [6] investigated the elastic deformations of foams and presented efficient formulae for the effective elastic moduli. However, the inelastic deformation behaviour of highly porous materials can be complex, depending strongly on the topology of the foam structure. Isotropic, kinematic and distortional hardening can occur. Consequently, the formulation of a closed form constitutive model is a very challenging task. In this work, an adaptable yield surface function is used, to capture the complex inelastic deformation behaviour and the large number of influence parameters (material and structural properties). The adaptable part of the proposed material model is represented by a neural network (NN).

NNs have been previously used in the literature to approximate material stiffness matrix [8, 9], strain energy density [10], drag stress for isotropic hardening and back stress for kinematic hardening of a given plasticity model [11] and for the identification of parameters of material laws [7, 12]. The great advantage of NNs is their adaptability to the given problem, but the generalization capability has to be checked to avoid over-fitting. The used NNs of this work are designed, trained and evaluated using the `python` library `ffnet` presented by Wojciechowski [7], see section 3.1.

2 FINITE ELEMENT MODEL OF A FOAM STRUCTURE

The simulation of whole foams requires very large meshes and enormous computational power based on their complexity. Consequently, representative volume elements (RVE), which are computationally more efficient, are often used for such simulations. During this work, a two dimensional (2D) structure is used, which is a simple 2D cross like structure consisting of four struts having the same length, as shown in Fig. 1.

The difference of the displacement vector between two homologous points at opposite boundaries $j+$ ($x_i^{j+} = l_{\mathrm{RVE}}/2$) and $j-$ ($x_i^{j-} = -l_{\mathrm{RVE}}/2$) of the 2D RVE is

$$\tilde{u}_i^{j+} - \tilde{u}_i^{j-} = \Delta\bar{u}_i^j = l_{\mathrm{RVE}}\,\bar{\varepsilon}_{ij} \tag{1}$$

with $i, j = 1, 2$, the macroscopic relative displacement $\Delta\bar{u}_i^j$ and the RVE size l_{RVE}. Additionally, the homogenized (macroscopic) stresses and strains are $\bar{\sigma}_{ij}$ and $\bar{\varepsilon}_{ij}$, which are the volume weighted averages of the microscopic stresses and strains $\tilde{\sigma}_{ij}$ and $\tilde{\varepsilon}_{ij}$

$$\bar{\sigma}_{ij} = \frac{1}{V_{\mathrm{RVE}}}\int \tilde{\sigma}_{ij}\mathrm{d}V, \qquad \bar{\varepsilon}_{ij} = \frac{1}{V_{\mathrm{RVE}}}\int \tilde{\varepsilon}_{ij}\mathrm{d}V, \tag{2}$$

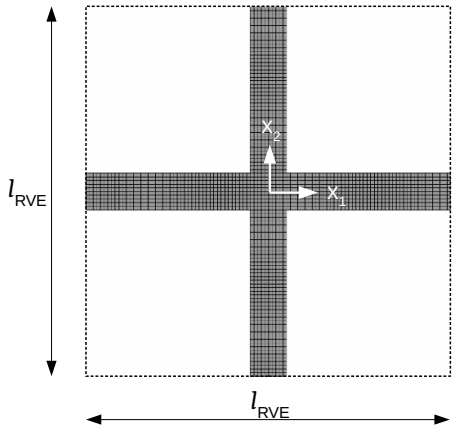

Figure 1: FE mesh for used 2D-model.

evaluated at reference nodes. The equilibrated microscopic tractions $\tilde{t}_j$ have opposite signs

$$\tilde{t}_i^{j-} = -\tilde{t}_i^{j+}. \tag{3}$$

More information about the used periodic boundary conditions and homogenization is given by Storm et al. [6].

3 NEURAL NETWORK FOR MODELLING PLASTIC DEFORMATIONS

In the following, an approach is described to model the macroscopic elastic-plastic deformation behaviour of foam structures by an adaptable yield surface using neural networks.

3.1 Neural network

Feed forward neural networks (FFNN) are used in the present study, where each network layer is fully connected to the directly preceding layer. The following layers are used: one input layer (with n nodes), one hidden layer (with m nodes) and one output layer (with k nodes), as depicted in Fig. 2. At all hidden and output layer nodes the sigmoid function

$$h(v_j) = \frac{1}{1 + e^{-v_j}} \tag{4}$$

is evaluated as activation function. Here, v_j is the nodal input value and represents the sum of the weights w_l of all connections l from the nodes of the preceding layer to node j and the bias b_j of this node

$$v_j = \sum_l w_l \, v_l + b_j. \tag{5}$$

To approximate a given data set, the free parameters of $n \cdot m + m \cdot k$ weights and $m + k$ biases have to be determined. This is done by minimizing the error function

$$err^{\text{train}} = \frac{1}{2} \sum_{p \in \mathcal{T}} \sum_i \left(val_i^{(p)} - \text{NN}_{\text{out}_i}^{(p)} \right)^2 \tag{6}$$

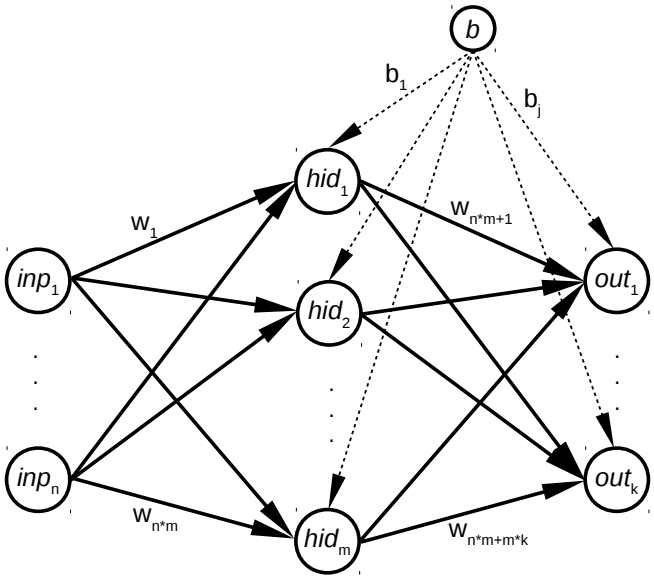

Figure 2: Structure of neural network (input layer with n nodes, one hidden layer with m nodes and output layer with k nodes with $i = n \cdot m + m \cdot k$ different weights w_i at solid arrows and $j = m + k$ different biases b_j at dashed arrows).

between the output of the NN and the given output data, with p as the unique input pattern of the training data set $\mathcal{T}$, val_i as the values of the training data and $\mathrm{NN}_{\mathrm{out}_i}$ as the output of the NN for the corresponding input pattern. This parameter optimization is called 'training' for NNs and is done using a Newton conjugate gradient algorithm based on the first derivative of the NN with respect to the weights. For the utilised `python` library `ffnet` [7], the training is done by the function `fmin_tnc` of the library `SciPy`.

One disadvantage of the training of NNs is the possibility of over-fitting. There are two different ways to avoid over-fitting while keeping a good approximation of the data set. First, the number of training pattern has to be greater than two times the number of free parameters of the NN

$$|\mathcal{T}| > 2 \cdot (n \cdot m + m \cdot k + m + k)\,. \tag{7}$$

The second way is a split of the data set $\mathcal{D}$ into the training data set $\mathcal{T} \subset \mathcal{D}$ and a separate set of evaluation data $\mathcal{E}$ with $|\mathcal{E}| \approx 10\%\,|\mathcal{D}|$, which are not part of the training set $\mathcal{E} = \overline{\mathcal{T}}$, see Fig. 3a. After each training step the error for $\mathcal{E}$ is calculated by Eq. (6). Finally, the weights and biases of the training step with the lowest $err_{\mathcal{E}}$ are used, see Fig. 3b.

3.2 Material modelling

For the description of the microscopic and macroscopic elastic-plastic material behaviour, respectively, it is assumed that the total strain ε_{ij} is the sum of the elastic $\varepsilon_{ij}^{\mathrm{el}}$ and plastic strains $\varepsilon_{ij}^{\mathrm{pl}}$

$$\varepsilon_{ij} = \varepsilon_{ij}^{\mathrm{el}} + \varepsilon_{ij}^{\mathrm{pl}} \tag{8}$$

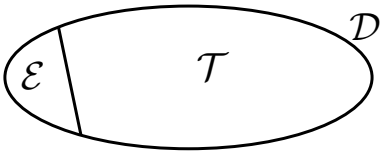

(a) Used data sets for training $\mathcal{T}$ and evaluation $\mathcal{E}$.

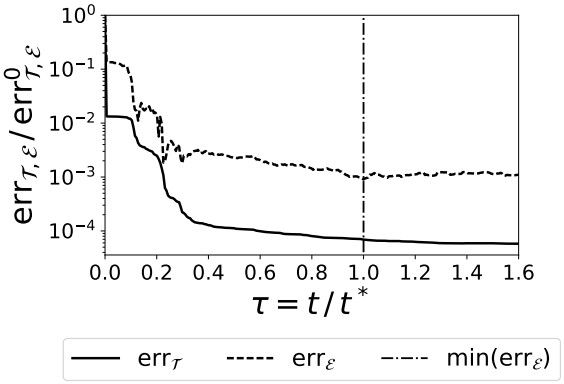

(b) Error of training data set $\mathcal{T}$ and evaluation data set $\mathcal{E}$ over training time (weights and biases of trained NN are used for $t = t^*$).

Figure 3: Different data sets and error values versus training time for neural network.

for small deformations. In addition, it is assumed that the stresses can be calculated by Hooke's law

$$\sigma_{ij} = C_{ijkl}\varepsilon^{\mathrm{el}}_{kl} = C_{ijkl}\left(\varepsilon_{kl} - \varepsilon^{\mathrm{pl}}_{kl}\right) \tag{9}$$

with C_{ijkl} as the stiffness tensor. The evolution of the plastic strains is described by the non-associated flow rule

$$\dot{\varepsilon}^{\mathrm{pl}}_{ij} = \xi \frac{\partial g}{\partial \sigma_{ij}} \tag{10}$$

whereby ξ is the plastic multiplier and g the plastic potential function. The model is complemented by a yield function $f(\sigma_{ij})$, which satisfies the loading-unloading condition

$$f \leq 0, \quad \xi \leq 0, \quad f \cdot \xi = 0. \tag{11}$$

In the present work, two different microscopic yield criteria are investigated in combination with isotropic linear elasticity (elastic modulus $\tilde{E}$ and Poisson's ratio $\tilde{\nu}$): The von Mises criterion with associated flow ($\tilde{g} \equiv \tilde{f}$) and the Drucker-Prager criterion with non-associated flow ($\tilde{g} \neq \tilde{f}$).

The yield function for both criteria has the form

$$\tilde{f}\left(\tilde{\sigma}_{ij}\right) = \tilde{q} + \alpha \tilde{I}_1 - (1-\alpha)\,\tilde{\sigma}_{\mathrm{Y}} \tag{12}$$

with the equivalent stress

$$\tilde{q} = \sqrt{\frac{3}{2}\left(\tilde{\sigma}_{ij} - \frac{1}{3}\tilde{I}_1\delta_{ij}\right)\left(\tilde{\sigma}_{ij} - \frac{1}{3}\tilde{I}_1\delta_{ij}\right)}, \tag{13}$$

the first stress invariant $\tilde{I}_1 = \tilde{\sigma}_{ii}$ of the microscopic stresses (planar stress state, based on 2D models in this work), the parameter α, and the yield stress $\tilde{\sigma}_{\mathrm{Y}}$. The plastic potential has the form

$$\tilde{g}\left(\tilde{\sigma}_{ij}\right) = \tilde{q} + \beta \tilde{I}_1, \tag{14}$$

with parameter β. For $\alpha = \beta = 0$ Eqs. (12) and (14) represent the von Mises criterion. In contrast, for $\alpha \neq 0$ Eq. (12) describes the Drucker-Prager criterion. Additionally, for the second criterion $\beta \neq \alpha$ is used for non-associated plasticity.

For both microscopic yield criteria, the Ludwik equation is chosen for the yield stress

$$\tilde{\sigma}_{\mathrm{Y}} = \tilde{\sigma}^0_{\mathrm{Y}} + \tilde{K} \left(\tilde{\varepsilon}^{\mathrm{pl}}_{\mathrm{eq}}\right)^{\tilde{n}} \tag{15}$$

with the microscopic equivalent plastic strain rate

$$\dot{\tilde{\varepsilon}}^{\mathrm{pl}}_{\mathrm{eq}} = \sqrt{\dot{\tilde{\varepsilon}}^{\mathrm{pl}}_{\mathrm{ij}} \dot{\tilde{\varepsilon}}^{\mathrm{pl}}_{\mathrm{ij}}} \tag{16}$$

and the hardening parameters $\tilde{K}$ and $\tilde{n}$. A schematic stress-strain curve is depicted in Fig. 4 using the Ludwik equation for the microscopic yield stress.

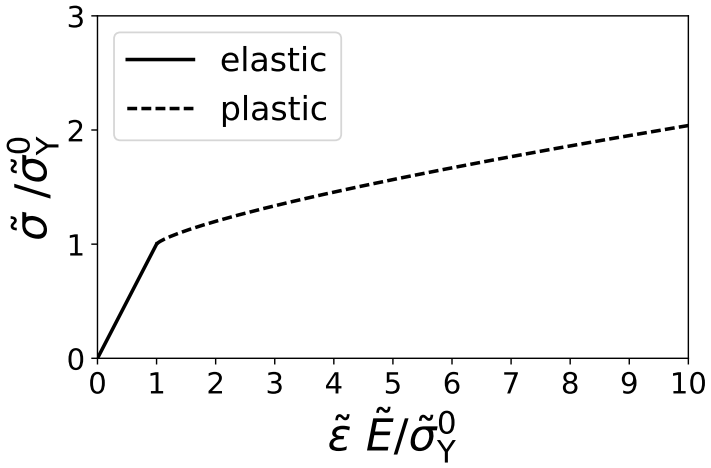

Figure 4: Scheme of elastic-plastic deformation for microscopic yield stress of Eq. (15) with $\tilde{K} = 0.2\,\tilde{E}$ and $\tilde{n} = 0.75$.

Now, the hybrid material model is described. Thereby, the term "macroscopic" refers to the description of the material model for testing the proposed model and additionally the deformation behaviour at the macroscopic scale for the foam structure. In particular, only proportional radial loading paths

$$\bar{\varepsilon}_{ij} = \lambda\, \bar{\varepsilon}^*_{ij}, \tag{17}$$

with the proportionality factor $\lambda \in \mathbb{R}^+_0$ and the macroscopic strain at initial microscopic yielding $\bar{\varepsilon}^*_{ij}$ are considered.

The macroscopic elastic deformation behaviour can be fully described by the tensor $\bar{C}_{ijkl}$. For the calculation of $\bar{C}_{ijkl}$, only three linear independent load cases are needed for a certain 2D structure, cf. the work of Storm et al. [6]. However, the consideration of the plastic foam behaviour is a great challenge, because $\bar{g}$, $\bar{f}$ and $\bar{\xi}$ have to be determined for each foam structure and strut material behaviour separately.

Javadi and Rezania [9] proposed a direct correlation between the macroscopic total strains and the resulting macroscopic stresses by NNs. In this approach, it is only possible to take into account elastic unloading successfully using a very complex neural network (many different input variables) to consider the loading history. With a more classical material modelling way, the form of a macroscopic yield function is postulated and the devoted material parameters are calculated for a good approximation. Now, a material modelling approach will be discussed using a more flexible yield function. The assumption is made that plastic deformations have no significant influence on the elastic deformation behaviour.

The macroscopic yield function is postulated to have the form

$$\bar{f}^{\mathrm{NN}}(\bar{\sigma}_{ij}) = \sqrt{\bar{\sigma}_{ij}\bar{\sigma}_{ij}} - \mathrm{NN}(\bar{I}_1, \bar{\varepsilon}^{\mathrm{pl}}_{\mathrm{eq}}) \tag{18}$$

with $\mathrm{NN}(\bar{I}_1, \bar{\varepsilon}^{\mathrm{pl}}_{\mathrm{eq}})$ as a neural network for the adaptable part to the specific form of the yield surface, depending on the first stress invariant $\bar{I}_1$ and the macroscopic equivalent plastic strain $\bar{\varepsilon}^{\mathrm{pl}}_{\mathrm{eq}}$. $\mathrm{NN}(\bar{I}_1, \bar{\varepsilon}^{\mathrm{pl}}_{\mathrm{eq}})$ is trained based on stress-strain curves with (microscopic) plastic deformations, cf. dashed line in Fig. 4, and its structure is depicted in Fig. 5.

The used yield function of Eq. (18) can represent the investigated microscopic yield criteria based on the chosen input variables of the NN: the first stress invariant and the equivalent plastic strain. The form of the yield function is not specified a priori like in the work of Furukawa and Hoffman [11]. Consequently, a wide range of plasticity models can be considered. The yield function of Eq. (18) used in this work captures only isotropic and distortional hardening. Based on monotonously proportional radial loading paths, it is not possible to measure kinematic hardening and so it is not considered here.

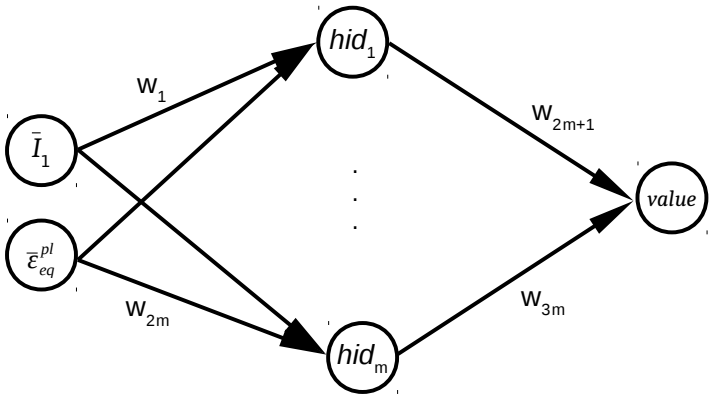

Figure 5: Structure of neural network $\mathrm{NN}(\bar{I}_1, \bar{\varepsilon}^{\mathrm{pl}}_{\mathrm{eq}})$ for adaptable yield surface of Eq. (18).

Correspondingly, the macroscopic flow rule, Eq. (10), becomes

$$\dot{\bar{\varepsilon}}^{\mathrm{pl}}_{ij} = \dot{\bar{\xi}} \frac{\partial \bar{f}^{\mathrm{NN}}}{\partial \bar{\sigma}_{ij}} = \dot{\bar{\xi}} \left(\frac{\bar{\sigma}_{ij}}{\sqrt{\bar{\sigma}_{kl}\bar{\sigma}_{kl}}} - \frac{\partial \mathrm{NN}(\bar{I}_1, \bar{\varepsilon}^{\mathrm{pl}}_{\mathrm{eq}})}{\partial \bar{I}_1} \delta_{ij} \right) \tag{19}$$

for associated plasticity ($\bar{g} = \bar{f}$) and

$$\dot{\bar{\varepsilon}}_{ij}^{\mathrm{pl}} = \bar{\xi} \frac{\partial \bar{g}}{\partial \bar{\sigma}_{ij}} \tag{20}$$

for non-associated plasticity. The quadratic (second order) norm gives

$$\left\| \dot{\bar{\varepsilon}}_{ij}^{\mathrm{pl}} \right\| = \sqrt{\dot{\bar{\varepsilon}}_{ij}^{\mathrm{pl}} \dot{\bar{\varepsilon}}_{ij}^{\mathrm{pl}}} = \bar{\xi} \sqrt{\frac{\partial \bar{g}}{\partial \bar{\sigma}_{ij}} \frac{\partial \bar{g}}{\partial \bar{\sigma}_{ij}}} = \bar{\xi} \left\| \frac{\partial \bar{g}}{\partial \bar{\sigma}_{ij}} \right\| \tag{21}$$

yielding

$$\dot{\bar{\varepsilon}}_{ij}^{\mathrm{pl}} = \underbrace{\left\| \dot{\bar{\varepsilon}}_{ij}^{\mathrm{pl}} \right\|}_{\bar{\xi}^* = \dot{\bar{\varepsilon}}_{\mathrm{eq}}^{\mathrm{pl}}} \frac{\frac{\partial \bar{g}}{\partial \bar{\sigma}_{ij}}}{\left\| \frac{\partial \bar{g}}{\partial \bar{\sigma}_{ij}} \right\|}. \tag{22}$$

Therein, $\frac{\partial \bar{g}}{\partial \bar{\sigma}_{ij}} / \left\| \frac{\partial \bar{g}}{\partial \bar{\sigma}_{ij}} \right\|$ are directions in the macroscopic strain space. This means, a second neural network is used for the consideration of the plastic flow vector for non-associated plasticity with the same structure as the NN for Eq. (18) based on an isotropic $\bar{g}$ ($\bar{I}_1$ and $\bar{\varepsilon}_{\mathrm{eq}}^{\mathrm{pl}}$ as input variables and values of the flow vector as output variables)

$$\frac{\frac{\partial \bar{g}}{\partial \bar{\sigma}_{ij}}}{\left\| \frac{\partial \bar{g}}{\partial \bar{\sigma}_{ij}} \right\|} = \mathrm{NN}(\bar{I}_1, \bar{\varepsilon}_{\mathrm{eq}}^{\mathrm{pl}}). \tag{23}$$

4 VERIFICATION WITH ANALYTICAL MATERIAL MODELS

To investigate the feasibility of the proposed hybrid material model based on an adaptable yield function, the elastic-plastic stress-strain curve is applied for two simple materials of the literature (von Mises and Drucker-Prager) with the Ludwik equation for the yield stresses, with $\tilde{K} = 0.2\,\tilde{E}$ and $\tilde{n} = 0.75$ in Eq. (15).

4.1 Associated von Mises plasticity

The von Mises yield criterion is evaluated for 19 different equispaced load paths in the principal strain space. The resultant stress-strain curves considering monotonic proportional loading (monotonously increase of proportional factor λ) are used for training of the adaptable yield function with $m = 40$ different nodes in the hidden layer of the neural network.

Afterwards, the stress-strain curves of the proposed hybrid model are compared with the results of the used elastic-plastic analytical model for three different loading paths with partial unloading. These stress-strain curves are depicted in Fig. 6.

If $\bar{\sigma}_{11}$ and $\bar{\sigma}_{22}$ have nearly the same magnitude, the agreement is very good, see Fig. 6a and b. But for the third loading path in Fig. 6c, the derivative of the yield function (for the plastic flow vector) has a small error. This fact can arise by fitting a function: only the function value itself is well represented, but not everywhere their derivative. Based on the error of the derivative and so for the calculated flow vector, these deviations accumulate. The flow vectors for the last increment of the third load case in Fig. 6 are given in Tab. 1.

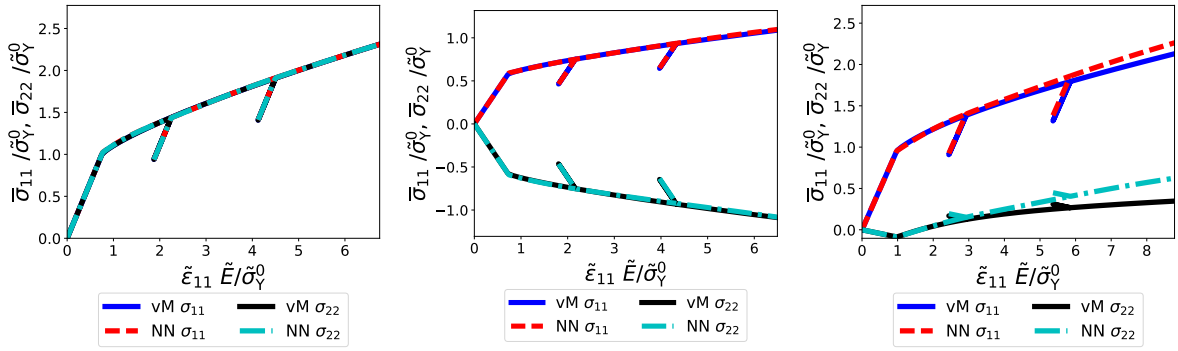

(a) $\bar{\varepsilon}_{22} = \bar{\varepsilon}_{11}$ (b) $\bar{\varepsilon}_{22} = -\bar{\varepsilon}_{11}$. (c) $\bar{\varepsilon}_{22} = -\frac{1}{3}\bar{\varepsilon}_{11}$.

Figure 6: Results for different load cases with von Mises (vM) criterion (associated plasticity).

Table 1: First derivatives of the flow potential for the analytical model (von Mises plasticity) and the hybrid model (calculated by Eq. (19)) at the last increment of the loading path in Fig. 6c.

	$\frac{\partial \bar{f}}{\partial \bar{\sigma}_{11}} / \left\lVert \frac{\partial \bar{f}}{\partial \bar{\sigma}_{ij}} \right\rVert$	$\frac{\partial \bar{f}}{\partial \bar{\sigma}_{22}} / \left\lVert \frac{\partial \bar{f}}{\partial \bar{\sigma}_{ij}} \right\rVert$	$\frac{\partial \bar{f}}{\partial \bar{\sigma}_{12}} / \left\lVert \frac{\partial \bar{f}}{\partial \bar{\sigma}_{ij}} \right\rVert$
analytical	0.9388	-0.3445	0
$\bar{f}^{\mathrm{NN}}$	0.9244	-0.3814	0

4.2 Non-associated Drucker-Prager plasticity

For the Drucker-Prager criterion the parameters $\alpha = \frac{1}{3}\tan 40°$ and $\beta = \frac{1}{3}\tan 20°$ are used to investigate non-associated plasticity. With this criterion 19 different monotonic loading paths are evaluated in the principal strain space and the stress-strain curves are used for the training of the hybrid yield surface and the direction of the plastic flow vector.

The stress-strain curves for this analytical model show an almost coincidence to each other for three different proportional loading paths with partial unloading, see Fig. 7.

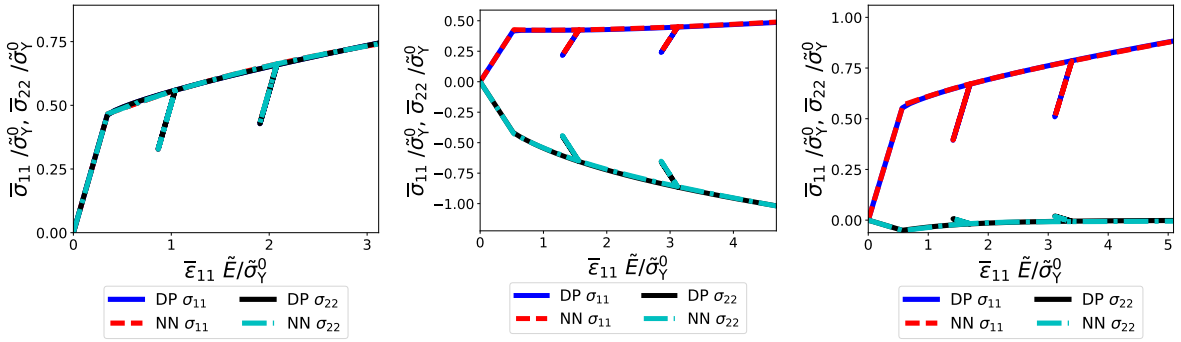

(a) $\bar{\varepsilon}_{22} = \bar{\varepsilon}_{11}$ (b) $\bar{\varepsilon}_{22} = -\bar{\varepsilon}_{11}$. (c) $\bar{\varepsilon}_{22} = -\frac{1}{3}\bar{\varepsilon}_{11}$.

Figure 7: Results for different load cases with Drucker-Prager (DP) criterion (non-associated plasticity).

5 RVE OF A FOAM STRUCTURE

The proposed material model is also applied for the elastic-plastic deformation behaviour of a simple foam structure shown in Fig. 1. For this RVE, numerical simulations are done using the FE code *ABAQUS* [13] with isotropic linear-elastic and isotropic ideal-plastic ($\tilde{K} = 0$ in Eq. (15)) material based on the von Mises criterion at the microscale. The plastic parts of the macroscopic stress-strain curves of 19 different equispaced monotonic loading paths in the macroscopic principal strain space are used for the training of both neural networks (one for the adaptable yield function and one for the direction of the flow vector). The plastic strains are calculated using Eq. (9) based on an assumed unloading. Both neural networks have $m = 40$ different nodes in the hidden layer.

Afterwards, three different loading paths ($\bar{\varepsilon}_{22} = \bar{\varepsilon}_{11}$, $\bar{\varepsilon}_{22} = -\bar{\varepsilon}_{11}$ and $\bar{\varepsilon}_{22} = -\frac{1}{3}\bar{\varepsilon}_{11}$) with partial unloading are evaluated using FE simulations with a fully discretized foam structure and using the proposed hybrid material model based on neural networks. The resultant stress-strain curves are depicted in Fig. 8.

All parts of the investigated stress-strain curves show a very good agreement. This means that the plastic deformations as well as the deformations during a partial unloading can be described very well with the proposed hybrid NN material model. It has to be noted, that the computational effort of the homogenized approach is drastically lower, cf. Tab. 2. It will be even better for 3D structures.

Table 2: Numerical effort of fully meshed foam structure and hybrid material model at the same computer for one load case of Fig. 8.

	fully meshed	NN
number of elements	1900	1
CPU time	390 s	2 s

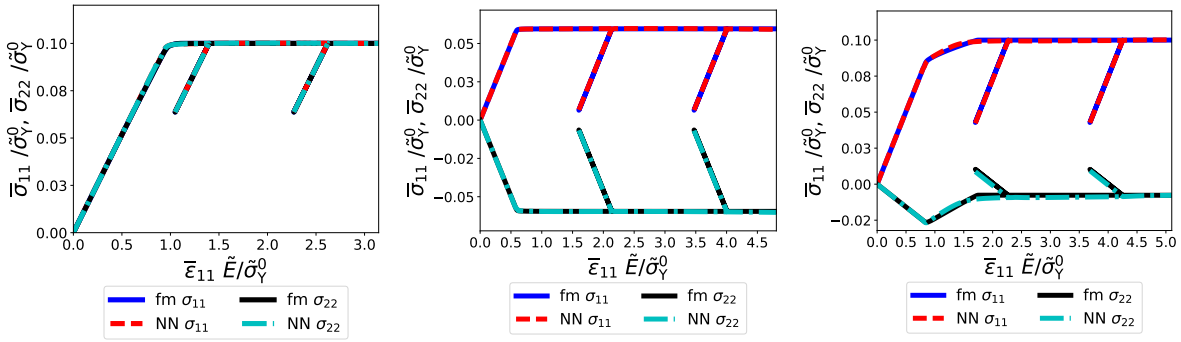

(a) $\bar{\varepsilon}_{22} = \bar{\varepsilon}_{11}$ (b) $\bar{\varepsilon}_{22} = -\bar{\varepsilon}_{11}$. (c) $\bar{\varepsilon}_{22} = -\frac{1}{3}\bar{\varepsilon}_{11}$.

Figure 8: Results for different load cases at foam structure (fully meshed (fm) and hybrid material model (NN)) with microscopic perfect von Mises plasticity ($\tilde{K} = 0$ in Eq. (15)).

The used foam structure has a very large anisotropic deformation behaviour. To take this fact into account, an extension is needed of the macroscopic yield function in Eq. (18).

6 CONCLUSIONS

In this research a hybrid constitutive material model for elastic-plastic deformation behaviours is developed. This hybrid model has an adaptable yield surface. It was verified using two different material models from the literature with associated and non-associated plasticity. Additional, it was applied to numerical homogenisation of the complex macroscopic elastic-plastic deformation behaviour of an open-cell foam structure. The numerical effort can be reduced essentially (by a factor of nearly 200) using the hybrid NN material model.

Ongoing research of the authors is aiming at an investigation of the deformation behaviour of foam filters using several RVEs. Therefore an increase of the number of the input variables for the neural networks is needed for macroscopic anisotropic yield surfaces and a formulation for the material tangent. Furthermore, it is possible to use the proposed approach to investigate 3D foam structures under 3D loadings by increasing the number of nodes per layer of the neural networks. Two open topics do remain: first, the verification of arbitrary loading directions (complex and non-proportional) and second, the applicability to finite deformations.

ACKNOWLEDGEMENTS

The authors gratefully acknowledge the financial support by the German Research Foundation (DFG) within the collaborative research centre SFB 920. Furthermore, the authors thank Mr. Wojciechowski as the developer of the open source `python` library `ffnet`.

REFERENCES

[1] Solarek, J., Himcinshi, C., Klemm, Y., Aneziris, C.G. and Biermann, H. Ductile behavior of fine-grained, carbon-bonded materials at elevated temperatures. *Carbon* (2017) **122**:141–149.

[2] Soltysiak, S., Abendroth, M., Kuna, M., Klemm, Y. and Biermann, H. Strength of fine grained carbon-bonded alumina (Al_2O_3–C) materials obtained by means of the small punch test. *Ceram. Int.* (2014) **40**:9555–9561.

[3] Wang, A.–J. and McDowell, D.L. Yield surfaces of various periodic metal honeycombs at intermediate relative density. *Int. J. Plast.* (2005) **21**:285–320.

[4] Storm, J., Abendroth, M. and Kuna, M. Geometry dependent effective elastic properties of open-cell foams based on Kelvin cell models. *Mech. Mater.* (2015) **86**:1–10.

[5] Demiray, S., Becker, W. and Hohe, J. Numerical determination of initial and subsequent yield surfaces of open-celled model foams. *Int. J. Solids Struct.* (2007) **44**:2093–2108.

[6] Storm, J., Abendroth, M., Zhang, D. and Kuna, M. Geometry dependent effective elastic properties of open-cell foams based on Kelvin cell models. *Adv. Eng. Mater.* (2013) **15**:1192–1298.

[7] Wojciechowski, M. Application of artificial neural network in soil parameter identification for deep excavation numerical model. *Comput. Assis. Mech. Eng. Sci.* (2011) **18**:303–311.

[8] Hashash, Y.M.A., Jung, S. and Ghaboussi, J. Numerical implementation of a neural network based material model in finite element analysis. *Int. J. Numer. Meth. Eng.* (2004) **59**:989–1005.

[9] Javadi, A.A. and Rezania, M. Intelligent finite element method: An evolutionary approach to constitutive modeling. *Adv. Eng. Inform.* (2009) **23**:442–451.

[10] Liang, G. and Chandrashekhara, K. Neural network based constitutive model for elastomeric foams. *Eng. Struct.* (2008) **30**:2002–2011.

[11] Furukawa, T. and Hoffman, M. Accurate cyclic plastic analysis using a neural network material model. *Eng. Anal. Bound. Elem.* (2004) **28**:195–204.

[12] Abendroth, M. and Kuna, M. Identification of ductile damage and fracture parameters from the small punch test using neural networks. *Eng. Fract. Mech.* (2006) **73**:710–725.

[13] Simulia Dessault Systemes *ABAQUS 6.12* (2012)